Formation and control of Turing patterns in a coherent quantum fluid

Vincenzo Ardizzone[1], Przemyslaw Lewandowski[2], M. H. Luk[3], Y. C. Tse[3], N. H. Kwong[3,4,5], Andreas Lücke[2], Marco Abbarchi[1,6], Emmanuel Baudin[1], Elisabeth Galopin[6], Jacqueline Bloch[6], Aristide Lemaitre[6], P. T. Leung[3,4], Philippe Roussignol[1], Rolf Binder[5,7], Jerome Tignon[1] & Stefan Schumacher[2,5]

[1]Laboratoire Pierre Aigrain, Ecole Normale Supérieure, CNRS (UMR 8551), Université Pierre et Marie Curie, Université D. Diderot, FR-75231 Paris Cedex 05, France, [2]Physics Department and Center for Optoelectronics and Photonics Paderborn (CeOPP), Universität Paderborn, Warburger Strasse 100, 33098 Paderborn, Germany, [3]Department of Physics, The Chinese University of Hong Kong, Hong Kong SAR, China, [4]Center of Optical Sciences, The Chinese University of Hong Kong, Hong Kong SAR, China, [5]College of Optical Sciences, University of Arizona, Tucson, AZ 85721, USA, [6]Laboratoire de Photonique et de Nanostructures, CNRS Route de Nozay, FR-91460 Marcoussis, France, [7]Department of Physics, University of Arizona, Tucson, AZ 85721, USA.

Nonequilibrium patterns in open systems are ubiquitous in nature, with examples as diverse as desert sand dunes, animal coat patterns such as zebra stripes, or geographic patterns in parasitic insect populations. A theoretical foundation that explains the basic features of a large class of patterns was given by Turing in the context of chemical reactions and the biological process of morphogenesis. Analogs of Turing patterns have also been studied in optical systems where diffusion of matter is replaced by diffraction of light. The unique features of polaritons in semiconductor microcavities allow us to go one step further and to study Turing patterns in an interacting coherent quantum fluid. We demonstrate formation and control of these patterns. We also demonstrate the promise of these quantum Turing patterns for applications, such as low-intensity ultra-fast all-optical switches.

Nonequilibrium patterns in open systems are ubiquitous in nature[1], with examples as diverse as desert sand dunes[2], animal coat patterns such as zebra stripes[3,4], or geographic patterns in parasitic insect populations[5]. Motivated by the quest to understand the chemical basis for morphogenesis, Turing proposed in 1952 a chemical reaction-diffusion model[6] that has been used to explain patterns in a diverse range of research fields[4,5,7–10]. Probably the most faithful realisation of Turing's original activator-inhibitor model was reported in chemical reactions by DeKepper and co-workers[11]. Important characteristics of these patterns include the fact that they are stationary, and the patterns' structure size is not dictated by the physical size of the system. Moreover, Turing structures occur in systems in which the spatially uniform phase is stable against uniform fluctuations; only spatially varying perturbations experience instability and growth, and thus contribute to spontaneous symmetry-breaking and pattern formation.

The definition of Turing patterns has been extended to optical systems, in which the spatial propagation is diffractive rather than diffusive[12,13]. Even though there is no direct optical analog to activator and inhibitor, the classification of optical patterns[14,15] in terms of Turing structures creates a useful perspective of the underlying unifying principles. By definition, they do not include spatially localised structures such as optical solitons[12,16,17].

A further generalisation of Turing patterns includes quantum fluids, as long as the aforementioned characteristics are preserved. The observation of the relatively simple Turing patterns in quantum fluids could complement the well-known other forms of patterns in quantum systems, such as Abrikosov lattices and vortex lattices in superfluids or Bose condensates in atomic and polaritonic systems[18–22] and the BCS phase in magnetic fields[23] (these are based on vortices and are not 'simple' patterns in the density profile of the macroscopic quantum state). Microcavity polaritons[24–41] – composite quasi-particles that are partly photonic partly electronic – seem ideally suited for the search of Turing patterns in quantum fluids: polaritons combine rather fundamental quantum mechanical characteristics of excitons with the benefits of light that allows for a straightforward excitation and read-out. Moreover, the many-particle interactions in exciton systems are particularly rich and give a spinor character to the polariton fluid[42,43].

Here we demonstrate experimentally and analyse theoretically formation and control of Turing patterns in a coherent quantum fluid of microcavity polaritons. Complementing our experiments and full numerical

simulations, we also discuss the underlying physics using results of a previous analysis on simplified models of the polariton scattering dynamics. However, we also identify fundamental differences: the polariton patterns we report show clear signatures only observable for patterns in a two-component spinor field. We identify these signatures and show that they can be traced back to spin-dependent polariton interactions beyond mean-field approximation. In our study, microcavity polaritons prove to be a suitable playground to explore and control quantum Turing patterns through selective optical excitation of specific wave-vector components in Fourier space; this is not possible in most other pattern-forming systems. We believe that these findings open the door to a much broader understanding and application (e.g., in all-optical switches) of Turing patterns at the quantum/classical interface as well as in purely quantum mechanical systems.

Results

Figure 1a shows the double-cavity that was specifically designed for our study. The system is based on two cavities mutually coupled through the Bragg mirror in the center. GaAs quantum-wells are embedded in both cavities. In each of the two cavities the light-field is coupled strongly to the fundamental exciton resonance of the quantum-wells such that polaritons[42] are formed (details are given in the Methods Section). The resulting dispersions of polaritons can be seen in the photoluminescence at low excitation density in Fig. 1b. A finite (in-plane) momentum corresponds to propagation under an oblique angle. Two lower-polariton branches (LPBs) are formed. In the nonlinear experiments below, we excite the upper of the two LPBs with a continuous-wave pump beam with frequency ω_P in normal incidence ($k_P = 0$) to the cavity.

With increasing pump intensity, the density of pump-induced polaritons at $k_P = 0$ increases and Coulomb scattering of polaritons occurs; mediated by the exciton fraction of the polariton quasi-particles[26]. In our setup, this scattering is most efficient when two polaritons at $k = 0$ scatter off each other to opposite in-plane momenta $\mathbf{k}$ and $-\mathbf{k}$ right onto resonance with the lowest polariton branch at pump frequency ω_P (cf. Fig. 1 b). Through their photonic component, the scattered polaritons then leave the cavity under a finite angle as indicated in Fig. 1a (the angle is determined by the pump frequency and polariton dispersion including nonlinear shifts[42]). The pairwise scattering of polaritons to $\mathbf{k}$ and $-\mathbf{k}$ at ω_P is the basic mechanism behind build-up of signals in Fourier-space at finite k. Above a certain pumping threshold intensity, the stimulated nature of the polariton scattering[26] leads to spontaneous symmetry breaking

with strong signals propagating at finite k, defining an emission cone about the propagation direction of the pump. This marks the onset of pattern formation.

Figure 2a shows the measured far-field emission (corresponding to the Fourier-plane picture discussed above) from the cavity with pump intensity above threshold. The threshold power is at about 150 mW and the experiments in Fig. 2 are at 195 mW. Detection is in reflection geometry. The pump is linearly polarised and detection is polarised perpendicular to the pump's polarisation state. In contrast to the emission cone (circle in the Fourier-plane) one may have expected, clearly evident in Fig. 2a is a hexagonal pattern. In Fig. 2b we show that, in coincidence with the observed hexagonal pattern in the far-field emission, a stationary hexagonal pattern is observed in the near-field emission (spatial resolution is about 0.6 μm). The stable near-field pattern underlines the fixed phase-relation of signals on the six different spots in the far-field once the pattern has formed and the phase has locked in. In a spatially homogeneous setup, the symmetry breaking driving the hexagon formation (instead of a ring pattern) is induced by the hexagon-specific higher-order nonlinear interaction process of polaritons illustrated and discussed in more detail below. It is worth noting that above threshold, the shape of the pattern observed does not sensitively depend on the excitation intensity. We observe that in Fig. 2 b the hexagons appear slightly distorted and misalignments between different hexagons occur. This is consistent with the finding in Fig. 2a, that the hexagon observed in the far-field is slightly distorted and smeared out in k-space. We reckon that spatially varying sample imperfections might be the cause as well as residual spherical aberration from our imaging setup. The patterns' orientation is not dominated by built-in anisotropy along crystallographic axes[44,45]. However, we note that we do see evidence of a structural anisotropy as the general appearance of the hexagon changes with its orientation.

The build-up of the hexagonal pattern in Fig. 2 can be regarded as a multi-step process: (i) The basic stimulated scattering of polaritons leading to off-axis signals on a ring in the Fourier plane (cf. discussion below). In the spinor polariton fluid, this scattering can either preserve the linear polarisation state of both scattered polaritons or turn both of their polarisations perpendicular to the pump's[46]. Being negatively detuned to the exciton, here this scattering is more efficient in the cross-linear channel. For the pump intensity in Fig. 2 only one mode, a cross-linearly polarised mode, is unstable (above threshold) such that this component dominates the emission for finite $\mathbf{k}$. This is the simplest possible scenario as competition
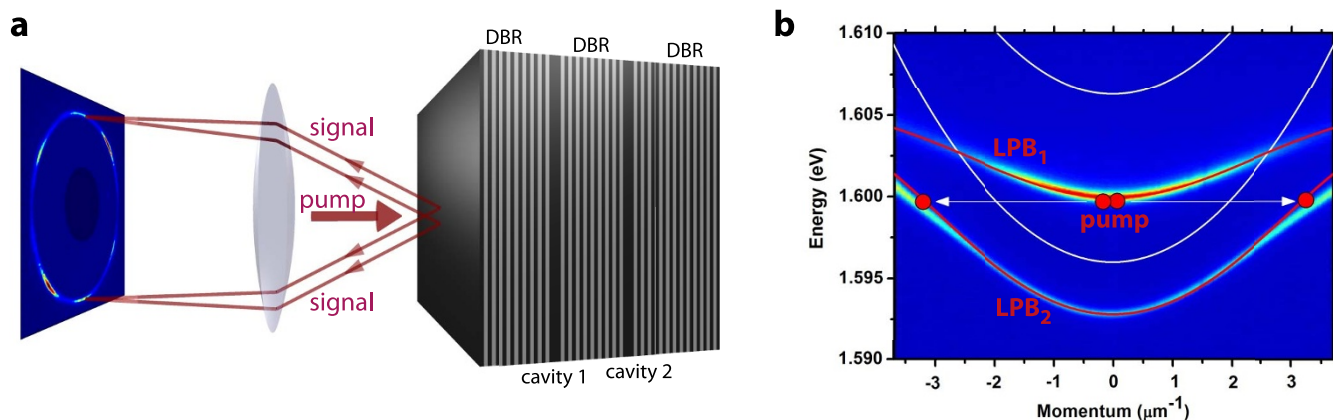

Figure 1 | The double-microcavity system. (a) Sketch of the double-microcavity and optical setup. The continuous-wave pump is in normal incidence to the DBRs (distributed Bragg reflectors). Signals are emitted under finite angle after spontaneous symmetry-breaking. Detection is in the Fourier-plane. (b) Measured luminescence showing the polariton dispersions at low density. The two lower-polariton branches LPB$_1$ and LPB$_2$ are visible. The theoretical bare cavity (white lines) and polariton (red lines) dispersions are included. The double-cavity design enables triply-resonant stimulated scattering of polaritons in this symmetric setup.
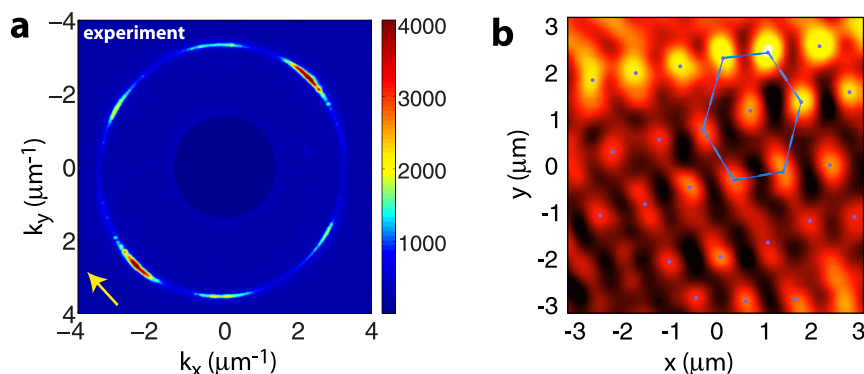
Figure 2 | Observation of hexagonal Turing patterns. Experimental (a) far-field and (b) near-field emission for linearly polarised continuous-wave pumping at k = 0 (yellow arrow gives pump polarisation state; detection is polarised perpendicular to the pump). Spontaneous hexagon formation is evident in (a) and (b). For clarity, in the detection, the signal is blocked out for small k. In the near-field image (b), as a guide to the eye the maxima in the extended hexagonal structure are marked and exemplarily one hexagon is highlighted.

between multiple unstable modes in different polarisation channels of the spinor polariton fluid (which would be an interesting aspect for future studies) is avoided. Additionally, the cross-linearly polarised excitation-detection setup is advantageous here as no direct stray light from the pump overshadows the desired signal in detection. (ii) Once the signals start growing at finite **k**, higher-order scattering processes[47] (see discussion below) couple different spots visible in the emission cone, leading to competition and further symmetry-breaking of its rotational invariance. (iii) The structure that self-stabilises as stationary behavior is approached, is a hexagon. This is the one structure for which the relevant higher-order nonlinear (in the finite-**k** polariton field amplitude; cf. discussion below) processes are phase-matched in our system that is dominated by a third-order nonlinearity[1,48]. Before we further elaborate on this point, however, we would like to demonstrate how the system behavior changes when spatial anisotropy is (intentionally) introduced.

Figure 3 shows the measured pattern when the pump is slightly tilted away from normal incidence ($k_{pump} \approx 0.1~\mu m^{-1}$). In this case, the optically induced anisotropy destabilises the hexagon and a transition into a stationary two-spot pattern is observed.

The control of transverse patterns with additional light beams has previously been used to realise a highly efficient all-optical switch in an atomic vapour[49–51]. Figure 4 shows the demonstration of an analogous all-optical switching with patterns in our microcavity system. The two-spot pattern at finite pumping angle is switched to a different orientation upon application of an extra light beam; cf. sketch in Fig. 4a. In panel **b** the two-spot pattern is oriented along the anisotropy axis induced by the pump. In panel **c**, without changing the

pumping configuration, the pattern has been steered away into the direction of an additional light beam sent into the system where the brightest spot is seen in the emission in **c**. This switching is reversed upon switching off the extra light beam. Our simulations discussed below indicate that the switching speed realistically achievable is on the tens of picoseconds timescale. We would like to emphasise that the extra beam (control beam) not merely induces additional conjugated spots (at **k** and −**k**) on the emission cone as one may have expected, but in this highly nonlinear system indeed steers away the pattern from its original orientation. A more detailed and dynamical investigation[52] of this pattern control (switching), we keep for a future study.

Discussion

To get a deeper insight into the mechanisms important for the pattern formation observed experimentally and discussed above, we have developed a theoretical description of the coupled cavity-field exciton dynamics inside the double-cavity system. The calculated data in Figs. 5 **a** and **b** are based on this full theory which is firmly based on the coherent nonlinear optical response of the fundamental excitons in the quantum wells derived from a microscopic semiconductor Hamiltonian[53–55]. We compute the dynamics of the excitonic fields self-consistently together with the optical fields in the cavities. The vectorial polarisation of the excitons and cavity fields and polarisation-dependent interactions are fully taken into account[46]. The system-specific parameters are obtained from a transfer-matrix modelling of the double-cavity system. The resulting linear dispersions are included in Fig. 1**b**. Full details about theory and numerical simulations are given in the Methods Section. We note that the numerical simulations cover the full two-dimensional plane such that all possible scattering processes are included and no restrictions to the topology of the stationary solutions and patterns formed are made. In these simulations, just as observed in the experiments, we find that for linear polarisation of the pump, a hexagon (over all the other possible patterns) spontaneously forms, which is oriented perpendicular to the axis defined by the pump's polarisation. The result is shown in Fig. 5a. As in the experiments, we also find two bright spots perpendicular to this axis and four spots reduced in intensity. Based on the calculations we could clarify that the reproducible pinning of the hexagon orientation to the pump's polarisation state is rooted in an interplay between the finite longitudinal-transverse (TE-TM) splitting of cavity modes (which is present in the experiments and included in the calculations) and the polarisation-dependent nonlinear interaction of the polaritons beyond mean-field approximation. The origin of a polarisation-induced spatial anisotropy can already be understood in the onset of pattern formation[56], however, here we report its manifestation also in the nonlinear regime, beyond the
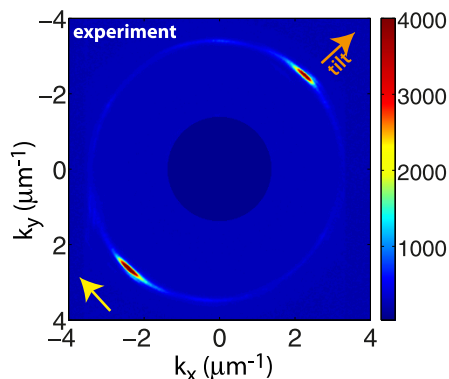

Figure 3 | Phase transition induced by spatial anisotropy. With the pump slightly tilted away from normal incidence, a two-spot pattern is observed.
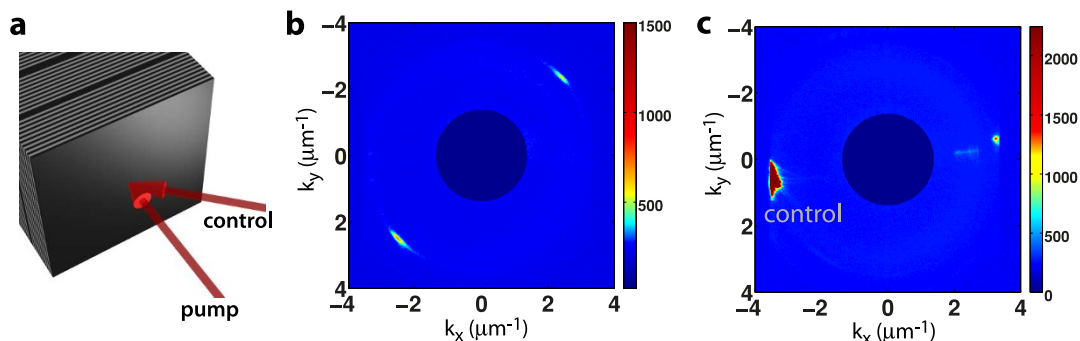
Figure 4 | Optical switching with patterns. (a) Sketch of the switching setup. (b) and (c) show spatial re-orientation of the two-spot pattern induced by an external control beam. The switching is reversed upon switching off the control.

analysis of linearly unstable modes. For excitation with a non-normally incident cw-pump, we find that instead of the hexagon a stable two-spot pattern is spontaneously formed (Fig. 5b). This result confirms our experimental observation that by optically introducing anisotropy into the system (by tilting the pump away from normal incidence), a transition from a hexagonal pattern to a two-spot pattern is induced. We classify the patterns we observe as generalised Turing patterns. They are stationary, the spatially homogenous state (represented by signals at $k = 0$) is stable while only $k \neq 0$ perturbations are unstable, and the pattern does not depend on the system's size (rather, it is determined by the pump frequency and polariton dispersion). In our polariton system, the system size can be varied with the size of the pump spot. The far-field patterns are indeed found to be similar in appearance for different pump spot sizes (not shown). In order to keep the changes at a minimum, the pump peak intensity, has to be slightly adjusted to compensate for the changes in the polariton walk-off from the pumping region for decreased or increased spot size. We note again that the diffusive transport in the original Turing pattern is replaced here by diffractive propagation of polaritons. The polariton interaction that leads to pattern formation is inherently quantum mechanical in nature: it is governed by the spin-dependent Coulomb interactions between the polariton's excitonic components and their underlying fermionic constituents.

The theoretical results presented above are based on direct simulations of the coupled, nonlinear, spinor cavity-field exciton dynamics inside the double-cavity system. On the other hand, the basic mechanism of the formation of hexagonal patterns (and subsets thereof) can be understood and explained by considering the individual effects and the interplay (competition and cooperation) of the polariton scattering processes shown in Fig. 6. By focussing on the

most relevant degrees of freedom, this alternative perspective allows a simpler analysis of the dynamics and a characterise of the system's quasi-stationary behaviour from a nonlinear dynamics viewpoint. In addition, it brings a close connection to the analyses of patterns in other systems[57], thus underlining the analogy of the polariton patterns to other systems showing pattern formation. A detailed analysis from this viewpoint was carried out in Ref. 58. In Ref. 58 we analysed the special case of a single cavity and the applied fields (pump and control) were limited to one circular polarisation, but the general arguments about hexagon formation invoked there hold for the more general case studied here. We briefly summarise in the following the essence of that analysis to make the present discussion more complete.

In the initial stage of pumping the microcavity with an on-axis ($k = 0$) intense beam, off-axis ($\mathbf{k} \neq 0$) polaritons are mainly generated through linear scatterings (Fig. 6a), where two pump polaritons scatter off each other into two opposite off-axis directions. Correspondingly, a linear analysis in the off-axis polariton field yields a modified dispersion relation for off-axis polaritons, which allows exponential growth for polaritons carrying transverse momenta lying within a certain window (close to the elastic circle on the renormalised polariton dispersion). As a matter of fact, only polariton modes with maximal linear growth rates dominate the subsequent scattering processes. Hence, instead of considering the entire range of $|\mathbf{k}|$, in a first approximation, only polariton modes within a narrow $|\mathbf{k}|$ range need to be retained in the analysis. In the absence of asymmetries induced by polarisation and/or imperfections of the cavity, the growth rate depends only on the magnitude of $\mathbf{k}$. Therefore, the modes actively participating in the pattern formation process all lie on a ring centered at the origin of the k-space. After pumping for a short while, the population of polariton
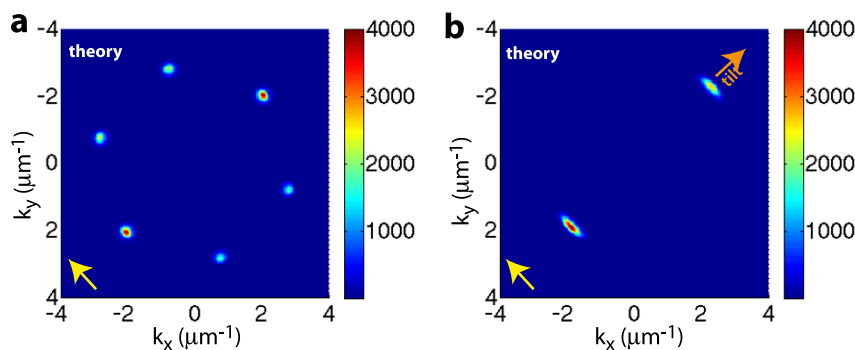

Figure 5 | Computed stationary patterns with and without spatial anisotropy. (a) Computed far-field emission for linearly polarised continuous-wave pumping at k = 0 (yellow arrow gives pump polarisation state; detection is polarised perpendicular to the pump). Spontaneous hexagon formation is evident. For clarity, detection is blocked out for small k. (b) Transition of the hexagonal pattern in (a) into a two-spot pattern when the pump is slightly tilted away from normal incidence along the direction marked by the orange arrow.
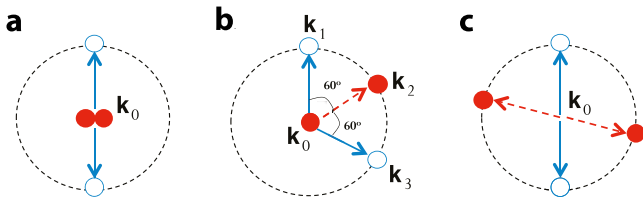
4

Figure 6 | Examples of phase-matched scattering. The scattering processes are specified by the incoming modes (red, solid circles) and outgoing modes (blue, open circles) in (transverse) momentum space. The arrows represent the modes' momenta, dashed (solid) for the incoming (outgoing) modes. The ring indicates the $\mathbf{k}$-space radius at which the polariton patterns reside. (a) Linear process: basic stimulated scattering at the origin of spontaneous symmetry breaking (pattern formation). (b) Quadratic process: momentum conservation is fulfilled only for modes arranged on a hexagon; it favors stabilisation of the hexagon. (c) Cubic process: cross-saturation leading to competition between pairs of phase-cunjugate modes.

modes on this k-space ring becomes so high that nonlinear scattering processes (Figs. 6b and c) take over the controlling role in the dynamics. A quadratic process contributing to the polariton dynamics in mode $\mathbf{k}_1$ is shown in Fig. 6b, where one off-axis polariton (from mode $\mathbf{k}_2$) and a pump polariton with zero momentum scatter into the modes $\mathbf{k}_1$ and $\mathbf{k}_3$. By (transverse) momentum conservation, quadratic processes such as this one are operative only among modes lying on the vertices of a regular hexagon. Their net effect was shown in Ref. 58 to tend to stabilise the hexagonal pattern. In an (azimuthally) isotropic setting, the orientation of the hexagon is arbitrary, and hence, if there were no further 'spontaneous' symmetry breaking mechanism, a ring composed of hexagons of all orientations would result. Such a mechanism is provided by the cubic processes, an example of which is shown in Fig. 6c. Generally serving to saturate the off-axis polariton growth, the cubic processes can be classified for our purpose into 'cross-saturating', as exemplified in Fig. 6c, and 'self- saturating' processes, where the outgoing modes are the same as the incoming ones. For polaritons, the cross-saturating processes exert a stronger effect than the self-saturating processes, favoring the tendency to form a spontaneously broken symmetry state[58]. Unlike the quadratic processes discussed above, the cubic processes do not require a hexagon geometry. Thus modes residing on different hexagons act on each other only through the cubic processes, leading to the broken-symmetry pattern of a single hexagon as observed in the simulations and the experiment. We note that, without this 'winner-takes-all' mechanism, small, unavoidable anisotropies present in the system would affect the ring pattern only perturbatively, and the ring would not collapse into a single stable hexagon.

In summary, in this Article we demonstrate formation and control of Turing patterns in a coherent quantum fluid of polaritons. In particular, we show that the Fourier components of the polariton patterns can selectively and efficiently be accessed all-optically (which is much more difficult in most other pattern-forming systems). This gives us control over the patterns. We show that the double-cavity we designed provides a suitable playground to study the complex phase-structure within and beyond the hexagonal patterns as well as for more general scenarios in a two-component spinor field. Apart from the fundamental interest, the exploration of the rich spectrum of instability and phase transitions could have implications for ultrafast polariton based all-optical switches[49–51]. For future studies also the quantum properties of the emitted light[59] with the possibility to study pattern-specific multi-mode quantum correlations would be of interest.

Methods

Experiments. The sample is formed by two λ/2 Al(0.95)Ga(0.05)As cavities. Distributed Bragg reflectors (DBR) are made by 25(back)-17.5(middle)-17.5(front)

couples of Al(0.95)Ga(0.05)As/Al(0.2)Ga(0.8)As layers. We deduce the theoretical finesse of the cavity of 9800 (in the case of zero absorption) from our transfer matrix simulations. The intermediate mirror permits coupling between the photonic modes of the two cavities, resulting in two modes at 1.596 eV and 1.606 eV separated in energy by 10 meV. Twelve quantum wells (QWs) are embedded in each cavity. The QW material is GaAs and each QW has a width of 7 nm. The exciton energy is at 1.6072 eV. A group of four QWs is placed in the centre of the cavity, at the anti-node of the electric field. Two other groups of four QWs are placed in the first couple of DBR layers. In such a structure strong coupling is easily achieved[44], resulting in two lower polariton branches (see Fig. 1b) and two upper polariton branches (not shown). The Rabi splitting is 13 meV. The rotation of the wafer was interrupted during MBE growth of the cavity spacer such that an intentional wedge is introduced. The resulting cavity gradient is about 2.6 meV/mm. This enables fine-tuning the photonic modes with respect to the excitonic modes by probing different points on the sample surface. All experimental data presented here refer to a slightly negative detuning.

For the optical experiments, the sample is held in a cold-finger cryostat at temperature of 6 K. Experiments are performed with a confocal setup. The laser is a Coherent MIRA Titan-Saphire laser. The pump spot size is 50 μm and the pump angle can be tuned finely. The excitation/detection optics is an inverted telescope ocular with a 16 mm working distance and large numerical aperture. The Fourier plane is imaged on the entrance slit of a 50 cm-long imaging spectrometer, equipped with a 1200 g/mm grating. A low noise charge coupled device (CCD) is used as detector for imaging. This system allows acquiring dispersion curves (as in Fig. 1) or images of the far field emission (with spectrometer entrance slit open and grating at zeroth order as in Figs. 2, 3, and 4).

Theory. Our theory is based on a microscopic density-matrix approach in the coherent limit for the excitonic polarisation inside the quantum wells coupled to the confined optical cavity fields in quasi-mode approximation[46]. We have adapted the theory to describe the double-cavity system and excitation scenario studied. The equations of motion then read as follows:

$$i\hbar \dot{E}_{\mathbf{k}}^{i\pm} = h_{\mathbf{k}}^i E_{\mathbf{k}}^{i\pm} + d_{\mathbf{k}}^{i,\pm} E_{\mathbf{k}}^{i\mp} - \Omega^i p_{\mathbf{k}}^{i\pm} - \Delta_C E_{\mathbf{k}}^{j\pm} + E_{\mathbf{k},inc}^{eff,\pm},$$

$$i\hbar \dot{p}_{\mathbf{k}}^{i\pm} = (\varepsilon_{\mathbf{k}}^{x,i} - i\gamma_x^i) p_{\mathbf{k}}^{i\pm} - \Omega^i E_{\mathbf{k}}^{i\pm}$$
$$+ \sum_{\mathbf{q}\mathbf{k}'\mathbf{k}''} \left(2\tilde{A}\Omega^i p_{\mathbf{q}}^{i\pm *} p_{\mathbf{k}'}^{i\pm} E_{\mathbf{k}''}^{i\pm} + T^{\pm\pm} p_{\mathbf{q}}^{i\pm *} p_{\mathbf{k}'}^{i\pm} p_{\mathbf{k}''}^{i\pm} \right. \tag{1}$$
$$\left. + T^{\pm\mp} p_{\mathbf{q}}^{i\mp *} p_{\mathbf{k}'}^{i\pm} p_{\mathbf{k}''}^{i\mp} \right) \delta_{\mathbf{q},\mathbf{k}'+\mathbf{k}''-\mathbf{k}},$$

with the in-plane momentum $\mathbf{k}$ of the respective field components. The index $+,-$ distinguishes the polarisation states in a circular basis. The upper index $i \neq j$ refers to quantities local in either of the cavities. The inter-cavity coupling is through the optical field with strength $2\Delta_C = 10$ meV and the exciton-photon Rabi splitting is $2\Omega^i = 13$ meV. The dispersion of the optical fields contains diagonal $h_{\mathbf{k}}^i = \frac{\hbar^2 k^2}{4}$ $(\frac{1}{m_L} + \frac{1}{m_T}) - i\gamma_c^i$ and off-diagonal elements $d_{\mathbf{k}}^{i,\pm} = -\frac{\hbar^2}{4}(\frac{1}{m_L} - \frac{1}{m_T})(k_y + ik_x)^2$ to account for TE-TM splitting with effective mass parameters $m_L = 3.79 \times 10^{-5} m_0$ and $m_T = 3.98 \times 10^{-5} m_0$ (with the electron mass m_0) for longitudinal and transverse components, respectively. For simplicity, the exciton dispersion $\varepsilon_{\mathbf{k}}^{x,i}$ was assumed to be constant. Decay of photons and exciton decoherence were set to $\gamma_c^i = \gamma_x^i = 0.2$ meV. The theory includes phase-space filling from the underlying fermionic character of excitations, with the matrix element $2\tilde{A} = 5.188 \cdot 10^{-4} \mu m^2$, and excitonic interaction through scattering matrices in equal and opposite spin channels, $T^{\pm\pm}$ and $T^{\pm\mp}$, respectively. We neglect quantum memory contributions[60] and the dispersive nature of the interactions for the largely monochromatic scenarios studied here. The values used at two times the pump frequency are $T^{\pm\pm}(2\omega_P) = V_{HF} = 5.69 \cdot 10^{-3}$ meVμm², for simplicity approximated by its Hartree-Fock value, and $T^{\pm\mp}(2\omega_P) = -T^{\pm\pm}(2\omega_P)/3$. Imaginary parts of T^{ij} are safely neglected at the large negative detunings studied. We further assume that for the relevant $\mathbf{k}$, the interactions and coupling constants Ω^i and Δ_C are k-independent. We solve the Fourier-transform of Eq. (1) directly on a finite-sized grid in real-space in two dimensions. The dispersion parameters were extracted from a comparison of the resulting linear dispersions with a transfer matrix modelling of the double-cavity structure.

1. Cross, M. C. & Hohenberg, P. C. Pattern formation outside of equilibrium. *Rev. Mod. Phys.* **65**, 851–1112 (1993).
2. Bowman, C. & Newell, A. Natural patterns and wavelets. *Rev. Mod. Phys.* **70**, 289–302 (1998).
3. Meinhardt, H. *Models of Biological Pattern Formation* (Academic Press, London, 1982).
4. Murray, J. *Mathematical Biology - II: Spatial Models and Biomedical Applications* (Springer, New York, 2003).
5. Hassell, M., Comins, H. & May, R. M. Spatial structure and chaos in insect population dynamics. *Nature* **353**, 255–258 (1991).
6. Turing, A. The chemical basis for morphogenesis. *Phil. Trans. R. Soc. Lond. B* **237**, 37–72 (1952).
7. Ball, P. *The self-made tapestry: Pattern formation in nature* (Oxford University Press, New York, 1999).

8. Epstein, I. R. & Pojman, J. A. *An introduction to nonlinear chemical dynamics: oscillations, waves, patterns, and chaos* (Oxford University Press, New York, 1998).

9. Koch, A. & Meinhardt, H. Biological pattern formation: from basic mechanisms to complex structures. *Reviews of Modern Physics* **66**, 1481–1507 (1994).

10. Penner, K., Ermentrout, B. & Swignon, D. Pattern formation in a model of acute inflammation. *J. Appl. Dyn. Syst.* **11**, 629–660 (2012).

11. Castets, V., Dulos, E., Boissonade, J. & De Kepper, P. Experimental evidence of a sustained standing Turing-type nonequilibrium chemical pattern. *Phys. Rev. Lett.* **64**, 2953–2956 (1990).

12. Staliunas, K. Three-dimensional Turing structures and spatial solitons in optical parametric oscillators. *Phys. Rev. Lett.* **81**, 81–84 (1998).

13. Oppo, G.-L. Formation and control of Turing patterns and phase fronts in photonics and chemistry. *J. Math. Chem.* **45**, 95–112 (2009).

14. Vaupel, M., Maitre, A. & Fabre, C. Observation of pattern formation in optical parametric oscillators. *Phys. Rev. Lett.* **83**, 5278–5281 (1999).

15. D'Alessandro, G. & Firth, W. J. Spontaneous hexagon formation in a nonlinear optical medium with feedback mirror. *Phys. Rev. Lett.* **66**, 2597–2600 (1991).

16. Amo, A. *et al.* Polariton superfluids reveal quantum hydrodynamic solitons. *Science* **332**, 1167–1170 (2011).

17. Sich, M. *et al.* Observation of bright polariton solitons in a semiconductor microcavity. *Nature Photon.* **6**, 50–55 (2012).

18. Schweikhard, V., Coddington, I., Engels, P., Tung, S. & Cornell, E. A. Vortex-lattice dynamics in rotating spinor Bose-Einstein condensates. *Phys. Rev. Lett.* **93**, 210403 (2010).

19. Borgh, M. O., Keeling, J. & Berloff, N. G. Spatial pattern formation and polarization dynamics of a nonequilibrium spinor polariton condensate. *Phys. Rev. B* **81**, 235302 (2010).

20. Grosso, G., Nardin, G., Morier-Genoud, F., Leger, Y. & Deveaud-Pledran, B. Soliton instabilities and vortex street formation in a polariton quantum fluid. *Phys. Rev. Lett.* **107**, 245301 (2011).

21. Tosi, G. Geometrically locked vortex lattices in semiconductor quantum fluids. *Nature Comm.* **3**, 1243 (2012).

22. Carusotto, I. & Ciuti, C. Quantum fluids of light. *Rev. Mod. Phys.* **85**, 299–366 (2013).

23. Hoffman, J. E. *et al.* A four unit cell periodic pattern of quasi-particle states surrounding vortex cores in $Bi_2Sr_2CaCu_2O_{8 + \delta}$. *Science* **295**, 466–469 (2002).

24. Kuwata-Gonokami, M. *et al.* Parametric Scattering of Cavity Polaritons. *Phys. Rev. Lett.* **79**, 1341 (1997).

25. Fan, X., Wang, H., Hou, H. Q. & Hammons, B. E. Laser emission from semiconductor microcavities: The role of cavity polaritons. *Phys. Rev. A* **56**, 3233–3236 (1997).

26. Savvidis, P. G. *et al.* Angle-resonant stimulated polariton amplifier. *Phys. Rev. Lett.* **84**, 1547–1550 (2000).

27. Huang, R., Tassone, F. & Yamamoto, Y. Experimental evidence of stimulated scattering of excitons into microcavity polaritons. *Phys. Rev. B* **61**, R7854–R7857 (2000).

28. Ciuti, C., Schwendiman, P., Deveaud, B. & Quattropani, A. Theory of angle-resonant polariton amplifier. *Phys. Rev. B* **62**, R4825–R4828 (2000).

29. Stevenson, R. M. *et al.* Continuous wave observation of massive polariton redistribution by stimulated scattering in semiconductor microcavities. *Phys. Rev. Lett.* **85**, 3680–3683 (2000).

30. Malpuech, G., Kavokin, A., Langbein, W. & Hvam, J. M. Resonant Rayleigh scattering of exciton-polaritons in multiple quantum wells. *Phys. Rev. Lett.* **85**, 650–653 (2000).

31. Saba, M. *et al.* High-temperature ultrafast polariton parametric amplification in semiconductor microcavities. *Nature* **414**, 731–735 (2001).

32. Whittaker, D. M. Classical treatment of parametric processes in a strong-coupling planar microcavity. *Phys. Rev. B* **63**, 193305 (2001).

33. Langbein, W. Spontaneous parametric scattering of microcavity polaritons in momentum space. *Phys. Rev. B* **70**, 205301 (2004).

34. Savasta, S., Di Stefano, O., Savona, V. & Langbein, W. Quantum complementarity of microcavity polaritons. *Phys. Rev. Lett.* **94**, 246401 (2005).

35. Kasprzak, J. *et al.* Bose–Einstein condensation of exciton polaritons. *Nature* **443**, 409–414 (2006).

36. Keeling, J., Marchetti, F. M., Szymanska, M. H. & Littlewood, P. B. Collective coherence in planar semiconductor microcavities. *Semicond. Sci. Technol.* **22**, R1–R26 (2007).

37. Balili, R., Hartwell, V., Snoke, D. W., Pfeiffer, L. & West, K. Bose-Einstein Condensation of Microcavity Polaritons in a Trap. *Science* **316**, 1007–1010 (2007).

38. Utsunomiya, S. *et al.* Observation of Bogoliubov excitations in exciton-polariton condensates. *Nature Phys.* **4**, 700–705 (2008).

39. Tosi, G. *et al.* Vortex stability and permanent flow in nonequilibrium polariton condensates. *J. Appl. Phys.* **109**, 102406 (2011).

40. Deng, H., Haug, H. & Yamamoto, Y. Exciton-Polariton Bose-Einstein Condensation. *Rev. Mod. Phys.* **82**, 1489–1537 (2010).

41. Snoke, D. & Littlewood, P. Polariton Condensates. *Physics Today* **63**, 42 (2010).

42. Kavokin, A., Baumberg, J. J., Malpuech, G. & Laussy, F. P. *Microcavities.* Series on Semiconductor Science and Technology (Oxford University Press, USA, 2011).

43. Hivet, R. *et al.* Half-solitons in a polariton quantum fluid behave like magnetic monopoles. *Nature Phys.* **8**, 724–728 (2012).

44. Diederichs, C. *et al.* Parametric oscillation in vertical triple microcavities. *Nature* **440**, 904–907 (2006).

45. Abbarchi, M. *et al.* Discretized disorder in planar semiconductor microcavities: Mosaicity effect on resonant rayleigh scattering and optical parametric oscillation. *Phys. Rev. B* **85**, 045316 (2012).

46. Schumacher, S., Kwong, N. H. & Binder, R. Influence of exciton-exciton correlations on the polarization characteristics of polariton amplification in semiconductor microcavities. *Phys. Rev. B* **76**, 245324 (2007).

47. Buck, M. *et al.* Light-polarization and intensity dependence of higher-order nonlinearities in excitonic FWM signals. *Eur. Phys. J. B* **42**, 175–180 (2004).

48. Kheradmand, R., Sahrai, M., Tajalli, H. & Lugiato, L. A. All-optical switching in semiconductor microresonators based on pattern selection. *Eur. Phys. J. D* **47**, 107–112 (2008).

49. Dawes, A. M. C., Illing, L., Clark, S. M. & Gauthier, D. J. All-optical switching in Rubidium vapor. *Science* **308**, 672–674 (2005).

50. Dawes, A. M. C. *et al.* Transverse optical patterns for ultra-low-light-level all-optical switching. *Laser & Photon. Rev.* **4**, 221–243 (2010).

51. Schumacher, S., Kwong, N. H., Binder, R. & Smirl, A. L. Low intensity directional switching of light in semiconductor microcavities. *Phys. Status Solidi RRL* **3**, 10–12 (2009).

52. Saito, H., Aioi, T. & Kadokura, T. Order-disorder oscillations in exciton-polariton superfluids. *Phys. Rev. Lett.* **110**, 026401 (2013).

53. Kwong, N. H., Takayama, R., Rumyantsev, I., Kuwata-Gonokami, M. & Binder, R. Evidence of nonperturbative continuum correlations in two-dimensional exciton systems in semiconductor microcavities. *Phys. Rev. Lett.* **87**, 027402 (2001).

54. Kwong, N. H., Takayama, R., Rumyantsev, I., Kuwata-Gonokami, M. & Binder, R. Third-Order exciton-correlation and nonlinear cavity-polariton effects in semiconductor microcavities. *Phys. Rev. B* **64**, 045316 (2001).

55. Takayama, R., Kwong, N. H., Rumyantsev, I., Kuwata-Gonokami, M. & Binder, R. T-matrix analysis of biexcitonic correlations in the nonlinear optical response of semiconductor quantum wells. *Eur. Phys. J. B* **25**, 445–462 (2002).

56. Schumacher, S. Spatial anisotropy of polariton amplification in planar semiconductor microcavities induced by polarization anisotropy. *Phys. Rev. B* **77**, 073302 (2008).

57. Ciliberto, S., Coullet, P., Lega, J., Pampaloni, E. & Perez-Garcia, C. Defects in roll-hexagon competition. *Phys. Rev. Lett.* **65**, 2370–2373 (1990).

58. Luk, M. H. *et al.* Transverse optical instability patterns in semiconductor microcavities: polariton scattering and low-intensity all-optical switching. *Phys. Rev. B* **87**, 205307 (2013).

59. Ardizzone, V. *et al.* Bunching visibility of optical parametric emission in a semiconductor microcavity. *Phys. Rev. B* **86**, 041301 (2012).

60. Savasta, S., Di Stefano, O. & Girlanda, R. Many-body and correlation effects on parametric polariton amplification in semiconductor microcavities. *Phys. Rev. Lett.* **90**, 096403 (2003).

Acknowledgments

Author contributions

All authors have contributed to the presented work and took part in the discussion of the scientific results. Experiments were done at Ecole Normale Supérieure by V.A., M.A., E.B., P.R., J.T. Samples were grown at Laboratoire de Photonique et de Nanostructures by E.G., J.B., A.L. The theoretical work was done jointly by the Hong Kong (Y.C.T., M.H.L., P.T.L.), Tucson (N.H.K., R.B.), and Paderborn (P.L., A.L., S.S.) groups. The manuscript has been prepared by S.S., J.T., R.B. and N.H.K. All authors reviewed the manuscript.

Additional information